Sol-Gel Thin Film Formation

C. J. BRINKER,*1 A. J. HURD, G. C. FRYE, P. R. SCHUNK and C. S. ASHLEY

Sandia National Laboratories, Albuquerque, New Mexico 87185-5800, USA

ゾルゲル法による薄膜の形成

C. J. Brinker,*1 A. J. Hurd, G. C. Frye, P. R. Schunk and C. S. Ashley

Sandia National Laboratories, Albuquerque, New Mexico 87185-5800, USA

ディップ法（又はスピニング法）によるゾルゲル薄膜の形成は急激な溶媒の蒸発を伴った重力（又は遠心力）による溶媒の排出を含んでいる．ディップの途中で一定な膜厚プロファイルが形成され，そのプロファイルは構成溶液の蒸発速度や流れによって生じる表面張力の勾配によって決まる．ゾルに含まれている無機元素は溶媒の蒸発とともに濃縮され，膜形成プロセスの最後の段階で大きくなる毛細管力によって気液界面のメニスカスをゲル内部へ引き込みち密化される．生成膜の重要な特性である微構造（気孔率，表面積，気孔径）は無機元素の種類や大きさ，膜の生成途中での濃縮や蒸発の相対的な速度，毛細管力の大きさ，生成に伴うせん断力に依存している．

[Received April 12, 1991]

Sol-gel thin film formation by dipping (or spinning) involves gravitational (or centrifugal) draining accompanied by vigorous solvent evaporation. During dipping a steady-state film thickness profile develops, the shape of which is established by the evaporation rates of the fluid components and possible surface tension gradient driven flows. The entrained inorganic species are concentrated by the accompanying evaporation of solvent and compacted by capillary pressure developed at the final stage of the deposition process as liquid-vapor menisci recede into the gel interior. The important microstructural properties of the deposited film (% porosity, surface area, and pore size) depend on the size and structure of the inorganic species, the relative rates of condensation and evaporation during deposition, the magnitude of the capillary pressure, and the accompanying shear stress.

Key-words : *Sol-gel, Dip-coating, Spin-coating, Microstructure, Films*

1. Introduction

THIN films formed using sol-gel techniques represent the oldest commercial application of sol-gel technology. The first patent based on sol-gel processing was granted to Jenaer Glaswerk Schott & Gen. in 1939 for silicate sol-gel films formed by dip-coating.[1] Rear view mirrors produced by sol-gel thin film techniques have been in production since 1953, followed by antireflective (AR) coatings in 1964, and architectural coatings since 1969.[2),3)] Today sol-gel thin film coatings are being intensively studied for such diverse applications as protective and optical coatings (e. g., 4)-10)), passivation and planarization layers (e. g., 11)-13)), sensors (e. g., 14),15)), high or low dielectric constant films (e. g., 3),16),17)), inorganic mem-branes (e. g., 18),19)), electrooptic and non-linear optical films (e. g., 20)-22)), electrochromics (e. g., 23),24)), semiconducting anti-static coatings (e. g., 23)), superconducting films (e. g., 25)), strengthening layers (e. g., 26),27)), and ferroelectrics (e. g., 28),29).

Despite significant advances in technologies based on sol-gel thin film processing, there has been relatively little effort directed toward understanding the fundamentals of the sol-gel coating process itself. see (e. g., 30)-39)). This paper reports on recent studies that address the underlying physics and chemistry of sol-gel thin film formation by dip- (or spin-) coating. We first briefly review the aspects of sol-gel chemistry that govern the size and structure of the inorganic species which, along with the solvent(s), comprise the coating sol. We then discuss the salient features of dip- and spin-coating with consideration of single component fluids and binary fluid mixtures. We finally address the deposition of inorganic sols with regard to time scales and the effects of sol structure, capillary pressure, and the accompanying shear on such properties as refractive index, surface area, and pore size of the deposited films, which we measure using *in situ* techniques such as conventional and imaging ellipsometry[39)] and gas sorption on surface acoustic wave substrates.[14)] The goal of our research has been to establish generic schemes that enable tailoring of film microstructures to specific applications.

2. Sol-gel chemistry

The sol-gel process uses inorganic or metal organ-

*1 To whom correspondence should be addressed: Inorganic Materials Chemistry Division 1846, Sandia National Laboratories, Albuquerque, NM 87185-5800, USA

ic precursors.[40] In aqueous or organic solvents the precursors are hydrolyzed and condensed to form inorganic polymers composed of M-O-M bonds. For inorganic precursors (salts) hydrolysis proceeds by the removal of a proton from an aquo ion $[MO_NH_{2N}]^{z+}$ to form a hydroxo (M-OH) or oxo (M=O) ligand:

$$[MO_NH_{2N}]^{z+} + pH_2O \rightleftarrows [MO_NH_{2N-p}]^{(z-p)+} + pH_3O^+ \quad (1)$$

Condensation reactions involving hydroxo ligands result in the formation of bridging hydroxyl (M-OH-M) or bridging oxygen (M-O-M) bonds depending on the coordination number of M and the acidity of the bridging hydroxyl. Normally monomeric aquo cations are the only stable species at low pH and various monomeric or oligomeric anions the only species observed at high pH.[40] At intermediate pH, well-defined polynuclear ions are often the stable solution species (e. g., $[Zr_4(OH)_8(OH_2)_{16}]^{8-}$ or $[AlO_4Al_{12}(OH)_{24}(OH_2)_{12}]^{7-}$), but the metal solubility is normally limited there, usually leading to the precipitation of oxohydroxides, e.g., Al(O)OH[41] or Fe(O)OH,[42] or oxides, e.g., ZrO_2[43] or TiO_2.[44] If peptized by the addition of acid or sterically stabilized by adsorption of organic molecules, these colloidal sols are well-suited for film deposition by dipping.

The most commonly used organic precursors for sol-gel film formation are metal alkoxides ($M(OR)_z$), where R is an alkyl group (C_xH_{2x-1}).[40] Normally the alkoxide is dissolved in alcohol and hydrolyzed by the addition of water under acidic, neutral or basic conditions, although film formation is also possible by deposition of the neat alkoxides followed by exposure to moisture. Hydrolysis replaces an alkoxide ligand with a hydroxyl ligand:

$$M(OR)_z + H_2O \rightleftarrows M(OR)_{z-1}(OH) + ROH \quad (2)$$

Condensation reactions involving the hydroxyl ligands produce polymers composed of M-O-M or M-OH-M bonds plus, in most cases, the by-products water or alcohol as shown below for silicate condensation:

$$Si(OR)_3OH + Si(OR)_4 \rightleftarrows (RO)_3Si\text{-}O\text{-}Si(OR)_3 + ROH \quad (3)$$

$$2Si(OR)_3OH \rightleftarrows (RO)_3Si\text{-}O\text{-}Si(OR)_3 + H_2O \quad (4)$$

The reverse of reactions (3) and (4), viz., siloxane bond alcoholysis and siloxane bond hydrolysis, promote bond breaking and reformation processes that, if extensive, permit complete restructuring of the growing polymer.

Since metals of interest for sol-gel film formation (Si, Al, Ti, etc.) have coordination numbers (CN) ≥ 4, complete condensation would lead to compact, particulate oxides. In fact, for electropositive metals like Ti and Zr, it is difficult to avoid particle formation unless the alkoxide precursor is modified, e.g., chelated with slowly hydrolyzing multidentate ligands such as acetylacetonate (acac)[44] or alcohol amines,[45],[46] to reduce both the effective functionality[44] and the rates of hydrolysis and condensation.[44],[46] Silicon, however, is substantially less electropositive. Hydrolysis and condensation of silicon alkoxides occur at much lower rates and the condensation pathway can be more easily influenced by steric and chemical factors such as the steric bulk of the alkoxide ligand, the concentration of the acid or base catalyst, the molar ratio (r) of H_2O:M in Eq. (2), or the aging times (see, Figs. 1 and 2.[47],[48])

There is a considerable body of evidence based on

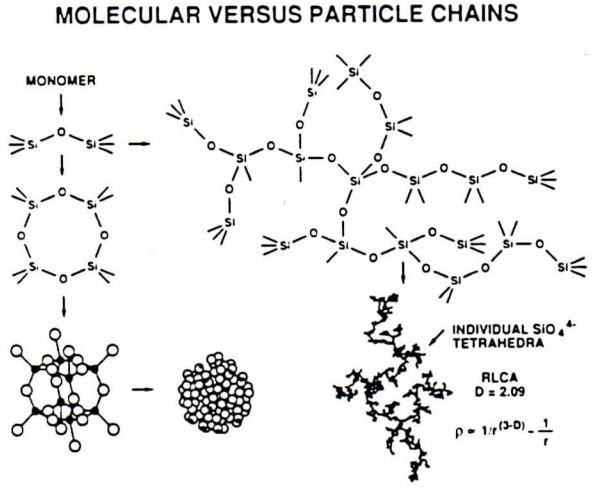

Fig. 1. Possible condensation pathways for silica polymerization. Aqueous conditions (or for metal alkoxides, high H_2O/Si), high pH, and/or high temperature promote the formation of compact, particulate structures. Low H_2O/Si, moderately acidic conditions, and low temperatures lead to more extended structures characterized by a mass fractal dimension D perhaps via reaction-limited cluster aggregation (RLCA).

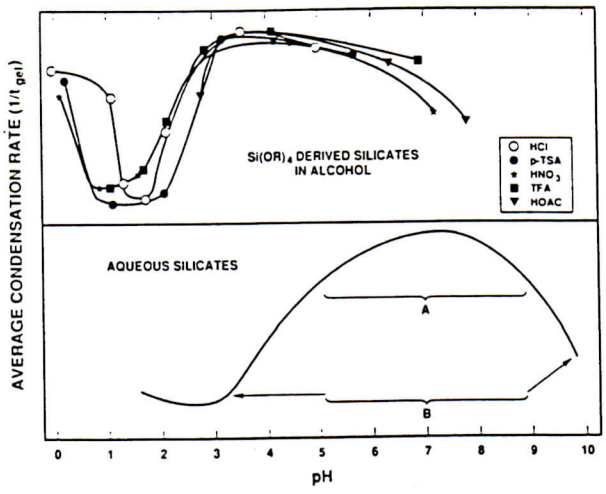

Fig. 2. Average condensation rates (estimated as $1/t_{gel}$) for silicates prepared from tetraethoxysilane (top) or for aqueous silicates[47] (bottom). Data in the top figure are from Coltrain et al.[48] where p-TSA is p-toluenesulfonic acid, HOAc, acetic acid; TFA, tri-fluoroacetic acid. In the bottom figure, A and B represent regions of high and low sticking probability, respectively.

^{29}Si NMR[49)-51)] and small-angle X-ray scattering (SAXS)[52)-54)] data indicating that, under many synthesis conditions, condensation of silicon alkoxides results in the formation of randomly branched "polymeric" silicates rather than dense silica particles. Silicate polymers are characterized using ^{29}Si NMR by the distribution of $Si(OR)_x(OH)_y(OSi)_n$ species, or Q^n distribution where $n=4-x-y$. The prevalence of Q^1–Q^3 species in Fig. 3[40)] clearly indicates that silicates may be very weakly condensed, compared, for example, to a commercial particulate silica sol.[47)]

SAXS probes structure on the ~0.5–50 nm length scale. The Porod slope, P, of a plot of log scattered intensity versus log scattering wave vector, $K=(4\pi/\lambda)\sin(\theta/2)$, is related to the mass fractal dimension, D, and the surface fractal dimension, D_s, by the following expression:[53)]

$$P=D_s-2D \qquad (5)$$

For uniform (non-fractal) objects $D=3$, $D_s=2$, and P reduces to -4. For mass fractal objects, $D=D_s$, and $P=-D$. For surface fractal objects, $D=3$ and $P=D_s-6$. Porod plots of a variety of silicates prepared from metal alkoxides are compared with the Porod plot of a commercial particulate silica sol in Fig. 4.[54)] It is generally believed[40)] that the prevalence of fractal silicates over a wide range of processing conditions is a consequence of kinetically limited growth mechanisms such as reaction-limited cluster-aggregation (RLCA).[55)]

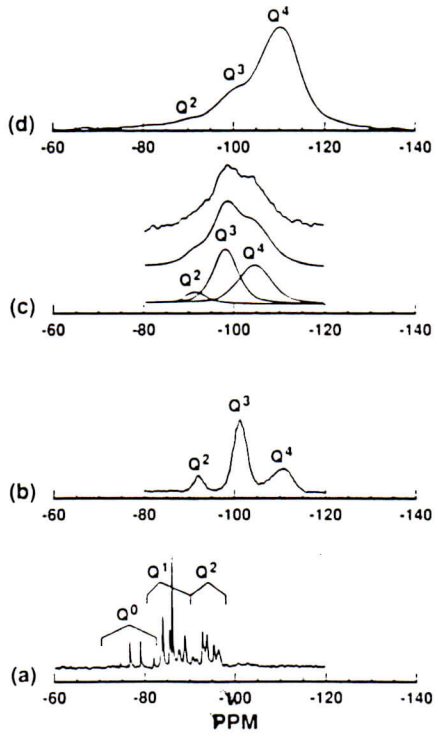

Fig. 3. Comparison of ^{29}Si NMR spectra of silicate sols prepared from tetraethoxysilane (TEOS) to the spectrum of a commercial aqueous silicate sol (LUDOX HS40).
(a) Acid-catalyzed TEOS sol ($H_2O/Si=2$) after three hours at room temperature;
(b) two-step acid-catalyzed TEOS sol ($H_2O/Si=5$);
(c) multicomponent silicate sol ($H_2O/Si=5$) aged for two weeks at 50°C and ~pH 3;
(d) LUDOX HS40.

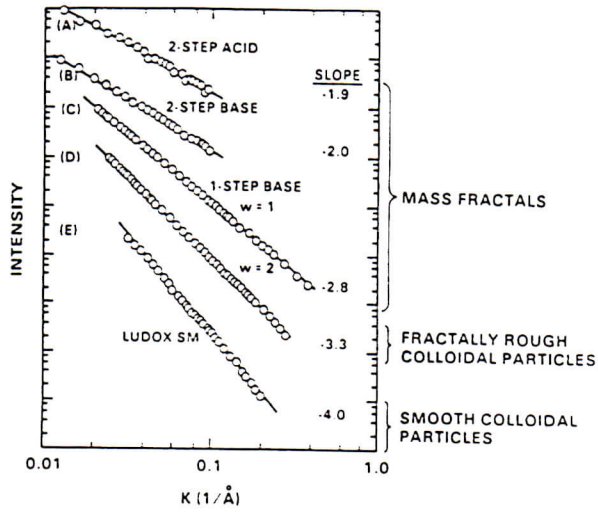

Fig. 4. Porod plots (log scattered intensity versus log scattering wave vector [$K=(4\pi/\lambda)\sin(\theta/2)$]) obtained by SAXS for a variety of silicate sols.
(A) two-step acid-catalyzed TEOS, (B) two-step acid-base catalyzed TEOS, (C) one-step base-catalyzed TEOS ($H_2O/Si=1$), (D) one-step base-catalyzed TEOS ($H_2O/Si=2$), and (E) commercial particulate silicate sol (LUDOX SM). From Schaefer and Keefer.[54)]

The mass fractal dimension D relates an object's mass M to its radius r:[56)]

$$M\sim r^D \qquad (6)$$

where for mass fractal objects, D is less than the dimension of space. The surface fractal dimension D_s relates an object's area A to its size:[56)]

$$A\propto r^{D_s} \qquad (7)$$

where in three dimensions $2\leq D_s\leq 3$. Since in three dimensions, $D<3$, the density of a mass fractal object decreases with distance from its center of mass:

$$\rho\propto 1/r^{(3-D)} \qquad (8)$$

Because density is inversely related to porosity, this relationship requires that, unlike Euclidian objects, fractal objects become more "porous" as their size increases. We will show that this property may be exploited to tailor the pore structure of films deposited from fractal precursors.

3. Film formation

3.1 Dip-coating

In dip-coating, the substrate is normally withdrawn vertically from the coating bath at a constant speed U_0 (see, Fig. 5a).[57)] The moving substrate entrains the liquid in a fluid mechanical boundary layer that splits in two above the liquid bath surface, returning the outer layer to the bath (see Fig. 5b).[38)] Since the solvent is evaporating and draining, the fluid film has an approximate wedge-like shape that terminates in a well-defined drying line ($x=0$, in Fig. 5a). When the receding drying line velocity

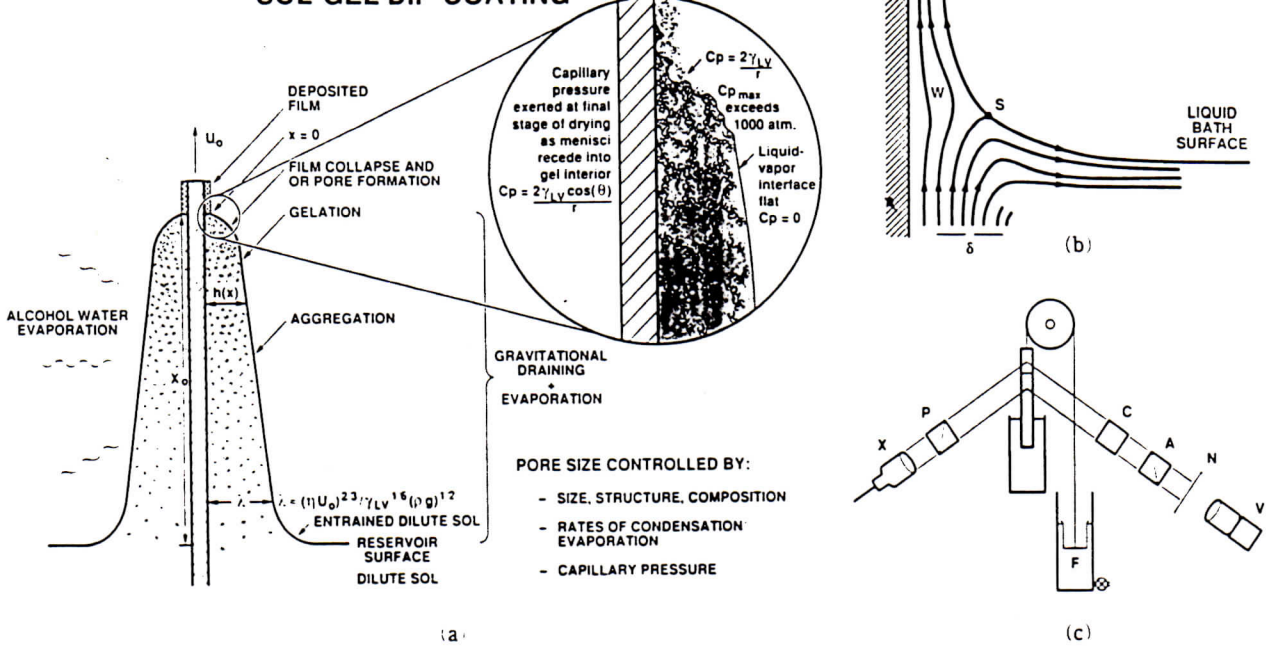

Fig. 5. (a) Schematic of the steady state dip-coating process, showing the sequential stages of structural development that result from draining accompanied by solvent evaporation and continued condensation reactions.
(b) Detail of liquid flow patterns (streamlines) during dip coating. U is the withdrawal speed, S is the stagnation point, δ is the boundary layer, and h is the thickness of the fluid film.
(c) Schematic of the imaging ellipsometer apparatus. Shaded area represents the sol reservoir and the entrained film. X is a beam expander; P a polarizer, C a quarter wave compensator; A an analyzer; N a diffusing screen; and V a video camera. From Hurd and Brinker.[39]

equals U_o, the process is steady state with respect to the liquid bath surface.[39]

The hydrodynamic factors in dip-coating (pure liquids, ignoring evaporation) were first calculated correctly by Landau and Levich[58] and recently generalized by Wilson.[59] In an excellent review of this topic, Scriven[38] states that the thickness of the deposited film is related to the position of the streamline dividing the upward and downward moving layers. A competition between as many as six forces in the film deposition region governs the film thickness and position of the streamline:[5] (1) viscous drag upward on the liquid by the moving substrate; (2) force of gravity; (3) resultant force of surface tension in the concavely shaped meniscus; (4) inertial force of the boundary layer liquid arriving at the deposition region; (5) surface tension gradient; and (6) the disjoining (or conjoining) pressure (important for films less than 1 μm thick).

When the liquid viscosity (η) and substrate speed are high enough to lower the curvature of the gravitational meniscus, the deposited film thickness (h) is that which balances the viscous drag ($\propto \eta U_o/h$) and gravity force ($\rho g h$):[38]

$$h = c_1(\eta U_o/\rho g)^{1/2} \qquad (9)$$

where the constant c_1 is about 0.8 for Newtonian liquids. When the substrate speed and viscosity are low (often the case for sol-gel film deposition), this balance is modulated by the ratio of viscous drag to liquid-vapor surface tension (γ_{LV}) according to the relationship derived by Landau and Levich:[58]

$$h = 0.94(\eta U_o)^{2/3}/\gamma_{LV}{}^{1/6}(\rho g)^{1/2} \qquad (10)$$

Figure 6 plots the logarithm of the product of thickness and refractive index*2 versus the logarithm of U_o for films prepared from a variety of silicate sols in which the precursor structures ranged from rather weakly branched polymers characterized by a mass fractal dimension to highly condensed particles.[57] The slopes are in the range 0.53 to 0.64, values bounded by the expectations from Eqs. (1) and (2).*3 This reasonable correspondence between the thicknesses of the deposited films and a theory developed for gravitational draining of pure fluids suggests that the entrainment of the inorganic species has little effect on the hydrodynamics of dip-coating, at least in the early stages of deposition where the entrained sol is quite dilute. Thus some insight into sol-gel film deposition may be gained by closer examination of the details of gravitational draining (and evaporation) of pure (and binary) fluids.

*2 Since the refractive index (n) is proportional to the volume fraction solids (ϕ), the product hn is proportional to the mass/unit area and takes into account the film porosity.

*3 As discussed in Section 4.3, the particulate sols appear to order at higher U_o, which may contribute to the lower slopes (0.53 and 0.58 compared to 0.62 and 0.64 observed for films prepared from polymeric sols).

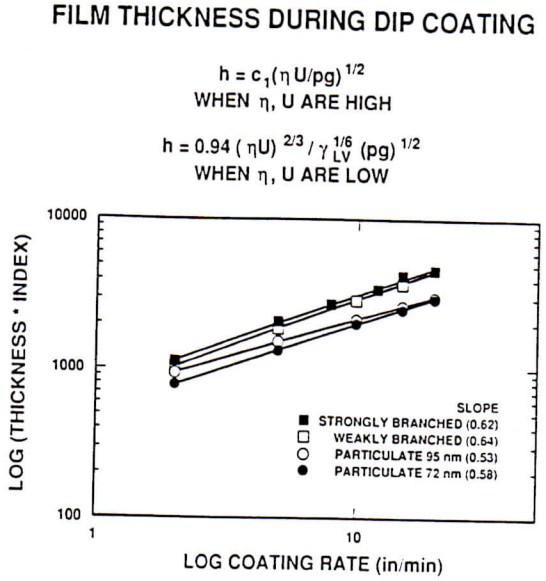

Fig. 6. Product of thickness and refractive index (proportional to film mass/unit area) versus withdrawal rate plotted according to Eqs. (9) or (10). From Brinker et al.[57]

3.2 Film thickness profiles during dip-coating: pure fluid

Previous theories of gravitational draining of pure fluids have not taken into account simultaneous evaporation. Although the thickness of the fluid entrained at the bath surface is apparently not sensitive to evaporation, the film is progressively thinned by evaporation as it is transported by the substrate away from the coating bath. For depositing sols, thinning by evaporation causes a corresponding increase in sol concentration, hence an understanding of simultaneous draining and evaporation is essential to the underlying physics of sol-gel film deposition.

In order to address this problem, Hurd and Brinker[39] developed an imaging ellipsometer that allows acquisition of spatially resolved thickness and refractive index data over the entire area of the depositing film (illustrated schematically in Fig. 5c). A thickness profile of an ethanol film obtained by imaging ellipsometry is shown in Fig. 7.[60] Instead of the wedge expected for a constant evaporation rate, the film profile is distinctly blunt near the drying line ($x=0$ in Figs. 5a and 7), which indicates more rapid thinning, and hence, a greater evaporation rate there.

The most significant factor in the rate of evaporation is the rate of diffusion of vapor away from the film surface. The blade-like geometry of the depositing film in the vicinity of the drying line led Hurd[60] to make an analogy between vapor diffusion (away from the film) and the electrostatic potential surrounding a knife blade, viz., the electric field at the surface is analogous to the evaporation rate (E) and the charge is analogous to the flux of vapor. Near any sharp boundaries, E diverges, but the vaporized mass must remain integrable. For the knife blade geometry (infinite sheet), E varies with x as follows:[60]

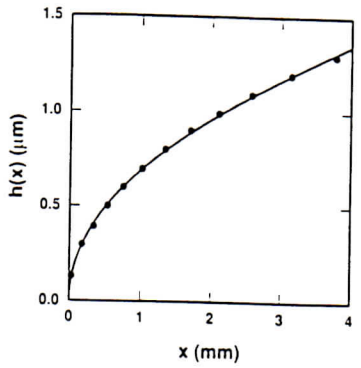

Fig. 7. Thickness profile of dip-coated ethanol film (solid dots). The profile is quite well fit by the form $h \sim x^{\nu}$ with $\nu = 0.50 \pm 0.01$ (solid line). From Hurd and Brinker.[60]

$$E(x) = -D_v a_1 x^{-1/2} \qquad (11)$$

where D_v is the diffusion coefficient of the vapor (~ 0.1 cm^2/s) and a_1 is a constant. Since thickness varies inversely with evaporation rate, the divergence in the evaporation rate as $x \to 0$ accounts for the blunt profile shown in Fig. 7, where the data are fit to the form:

$$h(x) \sim 1/E(x) \sim x^{\nu}, \quad \nu = 0.50 \pm 0.01 \qquad (12)$$

according to the expectations from Eq. (11).

The singularity strength (exponent) in Eq. (12) is sensitive to the geometry of the film. For coating a fiber, we would expect a logarithmic singularity,[61] and as a coated cylinder decreases in radius, the profile should pass smoothly from $x^{1/2}$ toward $\ln x$. Although some experimental evidence exists for this behavior by extrapolating to small cylinder diameters,[61] it is a difficult proposition to prove experimentally. Surface tension effects make it difficult to coat a fiber fast enough for the drying line to be well-separated from the gravitational meniscus at the reservoir surface.

3.3 Film fluid profiles during dip-coating: binary fluid

The most common coating sols are composed of two or more miscible liquids, e.g., ethanol-water. Differences in evaporation rates and surface tensions alter the shape of the fluid profile in the vicinity of the drying line*4 and create convective flows within the depositing film. Schunk[62] has developed a finite element model of the complete convective-diffusion problem associated with dip-coating an ethanol-water mixture. His strategy is to combine the theory of convection and diffusion in the liquid with a mass transfer model in the gas. Models and constitutive equations are used to account for liquid-vapor equilibria and surface tension. Thus far thermal effects induced by latent heat of evaporation and diffusion-driven convection are neglected*5 and

*4 In some cases rib-like instabilities are also observed in a region near the liquid bath surface.[61]

*5 Bornside et al.[63] have shown that for spin-coating with volatile solvents the temperature change of the depositing fluid is negligible (<1 K at 3000 rpm).

water is assumed to be relatively non-volatile. Conservation of mass and momentum (of both liquid and volatile species) leads to solutions for the position of the free surface (which locates according to the capillary hydrodynamic forces and ethanol loss by evaporation) and the concentration profiles and shown in Fig. 8.[62] Preferential evaporation of ethanol enriches the free (liquid-vapor) surface in water. In the vicinity of the drying line, the more volatile alcohol may be substantially depleted, leaving behind a water-rich film.

Corresponding ellipsometric images[61] of depositing alcohol-water films show two roughly parabolic features (Fig. 9), that correspond to successive drying of the alcohol- and water-rich regions, according to the non-constant evaporation model (Eq. (12)). This suggests that each component has an independent evaporation singularity. If the water-rich phase is denoted as phase 1 and ethanol is phase 2, then the independent profiles are additive:

$$h_1 = a_1 x^{1/2} \quad x > 0 \tag{13}$$

$$h_2 = a_2 (x - x_2)^{1/2} \quad x > x_2 \tag{14}$$

$$h_2 = 0 \quad x < x_2 \tag{15}$$

where h is the total thickness, and x_2 is the position of the "false" drying line created by the substantial depletion of ethanol.

The "foot" feature in Fig. 9 typical of binary solvents is not due to differential volatility alone. Since each component has a different surface tension γ, surface tension gradients are established:[61]

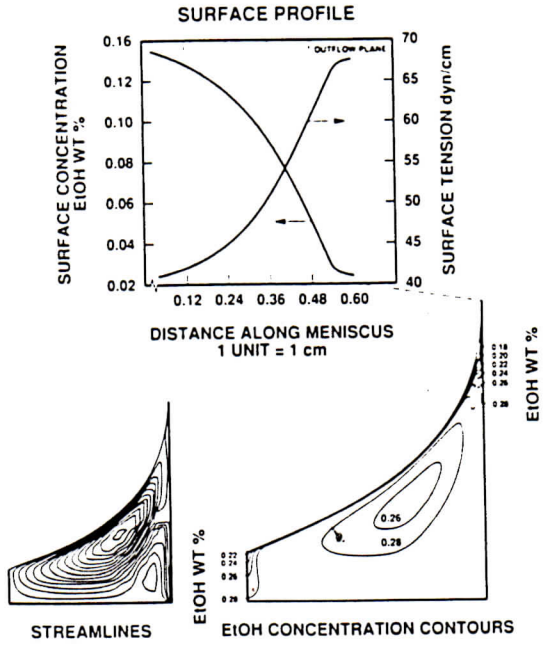

Fig. 8. Fluid streamlines and EtOH concentration contours of 30 wt% EtOH–70 wt% H_2O solution during dip-coating predicted by a finite element model. The overlying saturation of EtOH was assumed to vary linearly from 10% at the reservoir surface to 0% at the drying line. The change in ethanol concentration along the free (liquid-vapor) surface results in a steep gradient in surface tension. Substrate is represented in the bottom two plots by the vertical line on the right. From Schunk et al.[62]

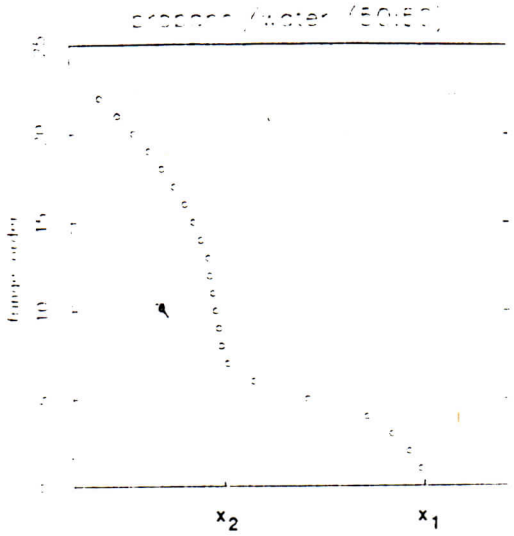

Fig. 9. Thickness profile of 50 : 50 propanol : water film (volume ratio). The double parabolic profile is due to differential volatilities and surface tension gradient driven flows. x_1 is the position of the drying line; x_2 is the position of the "false" drying line created by the depletion of the ethanol-rich phase. Film thickness equals approximately the fringe order times 240 nm. From Hurd.[61]

$$\begin{aligned} d\gamma/dx &= (\gamma_1 - \gamma_2)\, d\phi_1/dx \quad (x > x_2) \\ &= 0 \quad (0 < x < x_2) \end{aligned} \tag{16}$$

where the surface tension is assumed to follow a simple mixing law, $\gamma = \phi_1\gamma_1 + \phi_2\gamma_2$ where ϕ_i is the volume fraction of component i.*6 Since at the liquid-vapor boundary, the viscous shear force must balance the force imposed by surface tension gradients, $\eta du/dz = d\gamma/dx$ $(z = h)$, liquid flows into the water-rich foot with velocity u:

$$u = 1/\eta [d\gamma/dx] z - u_o, \tag{17}$$

the so-called "Marangoni effect". The foot slowly grows until this flux is balanced by that of evaporation from the expanding free surface.

The surface tension gradient driven flow of liquid through the thin neck created by the preferential evaporation of alcohol can create quite high shear rates during dip-coating. A striking example is that of toluene and methanol (see, Fig. 10).[61] The surface tension gradient driven flows are strong enough to greatly distort the double parabolic profile, creating a "pile-up" of toluene near the drying line. A crude estimate of the surface tension gradient, $\Delta\gamma/\Delta x \simeq ((10\ \text{dyne/cm})/10^{-1}\ \text{cm})$, leads to a shear rate, $du/dz \simeq 10^4\ \text{s}^{-1}$, in the thin region, from Eq. (17), assuming $\eta = 0.01$ P. As we discuss in Section 4.3, these shear fields may be sufficiently strong to align or order the entrained inorganic species.

3.4 Spin-coating

Spin-coating differs from dip-coating in that the

*6 For ethanol-water mixtures the surface tension does not obey a simple linear mixing law. The surface tension can be approximated by $1/(\gamma_{2.7}) \approx \phi_H/(\gamma_H^{2.7}) + \phi_E/(\gamma_E^{2.7})$ where the subscripts H and E refer to water and ethanol, respectively. (Terry Garino, private communication).

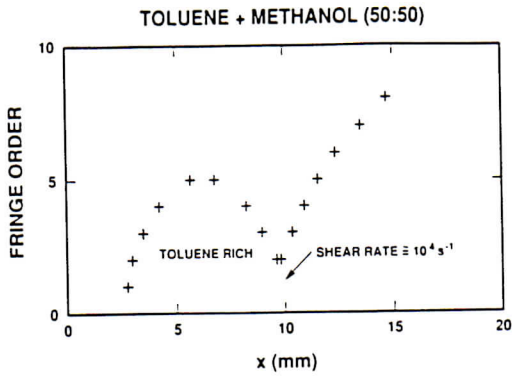

Fig. 10. Thickness profile of 50 : 50 methanol : toluene film (volume ratio). A steady state "bubble" of toluene forms due to strong surface-tension-gradient-driven flows. The thinning of the film creates a rather high shear rate. From Hurd.[61]

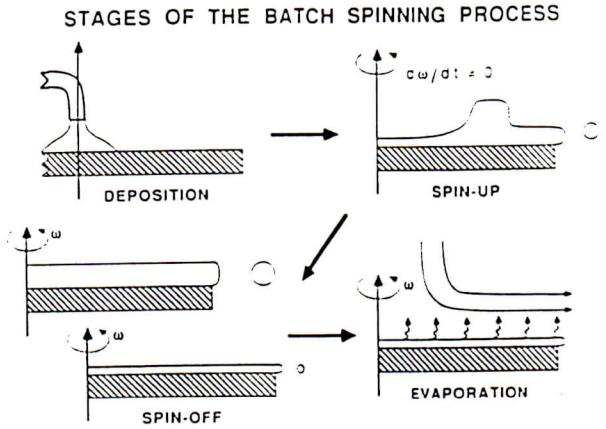

Fig. 11. The four stages of the batch spin-coating process. From Bornside et al.[63]

depositing film thins by centrifugal draining and evaporation (see, Fig. 11). Bornside et al.,[63] divide spin coating into four stages: deposition, spin-up, spin-off and evaporation, although for sol-gel coating, evaporation normally overlaps the other stages. An excess of liquid is dispensed on the surface during the deposition stage. In the spin-up stage, the liquid flows radially outward. driven by centrifugal force. In the spin-off stage excess liquid flows to the perimeter and leaves as droplets. As the film thins, the rate of removal of excess liquid by spin-off slows down, because the thinner the film, the greater resistance to flow, and because the concentration of the non-volatile components increases, raising the viscosity. In the final stage, evaporation takes over as the primary mechanism of thinning.

According to Scriven,[38] an advantage of spin-coating is that a film of liquid tends to become uniform in thickness during spin-off and, once uniform, tends to remain so provided that the viscosity is not shear-dependent and does not vary over the substrate. This tendency is due to the balance between the two main forces: centrifugal force, which drives flow radially outward, and viscous force (friction), which acts radially inward. The thickness of an initially uniform film during spin-off is described by:

$$h(t) = h_o/(1+4_{\rho\omega}{}^2 h_o{}^2 t/3\eta)^{1/2} \qquad (18)$$

where h_o is the initial thickness, t is time, ρ is the density, and ω is the angular velocity. Even films that are not initially uniform tend monotonically toward uniformity, sooner or later following Eq. (18).

Equation (18) pertains to Newtonian liquids that do not exhibit a shear rate dependence of the viscosity during the spin-off stage. If the liquid is shear-thinning (often the case for aggregating sols), the lower shear rate experienced near the center of the substrate causes the viscosity to be higher there and the film to be thicker. This problem might be avoided by metering the liquid from a radially moving arm during the deposition/spin-up stage.

3.5 Effects of condensed phases

The previous sub-sections have largely ignored the effects of the entrained inorganic species, viz., polymers or particles. These species are initially concentrated by evaporation of solvent as they are transported from the coating bath toward the drying line within the thinning fluid film during dipping or during the four stages of spin-coating. They are further concentrated (compacted) at the final stage of the deposition process by the capillary pressure C_p created by liquid-vapor menisci as they recede into the drying film (see, Fig. 5a):

$$C_p = 2\gamma\cos(\theta)/r_p \qquad (19)$$

where θ is the contact angle of the receding meniscus within the emptying pore and r_p is the pore size.

During dip-coating, the shape of the entrained fluid profile is altered very little by the presence of the condensed phase (see, Fig. 12a).[60] Thus by consideration of the conditions that establish the steady-state fluid profiles, we are able to quantify the changing environment of the inorganic species within the thinning film.

Above the stagnation point, all fluid elements are moving upward (see, Fig. 5b), so all the entrained inorganic species that survive past the stagnation point are incorporated in the final deposited film. Steady-state conditions in this region require conservation of non-volatile mass, thus the solids mass in any horizontal slice of the thinning film must be constant:[60]

$$h(x)\phi_s(x) = \text{constant} \qquad (20)$$

where ϕ_s is the volume fraction solids (see, Fig. 13a). From Eq. (20), we see that ϕ varies inversely with h. Since for a planar substrate there is a parabolic thickness profile, ϕ should vary as $1/h \simeq x^{-1/2}$ in the thinning film (see, Fig. 12b). When coating a fiber, we expect $\phi(x) \sim (\ln x)^{-1}$.

The rapid concentration of the entrained inorganic species by evaporation is more evident from consideration of the mean particle (polymer) separation distance $\langle r \rangle$, which varies as the inverse cube root of ϕ, $\langle r \rangle \sim x^{1/6}$. As shown in Fig. 13b,[61] this is a very

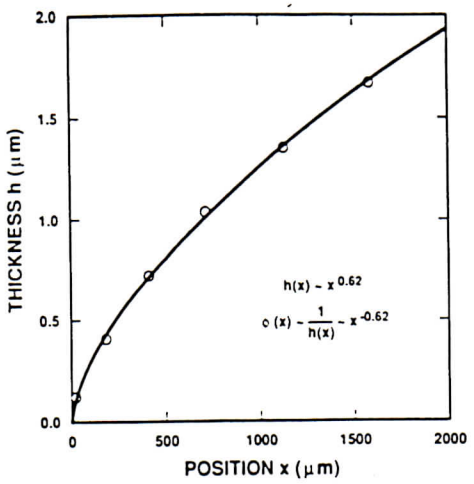

Fig. 12a. Thickness profile of a titanate sol during dip-coating as determined by imaging ellipsometry. Position x is defined in Fig. 5a. From Brinker et al.[37]

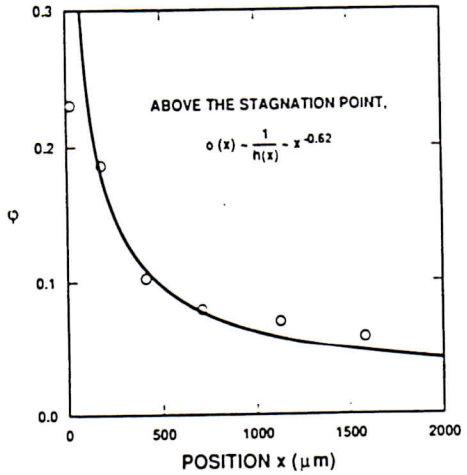

Fig. 12b. Volume fraction solids (ϕ) of the titanate sol versus position x as determined from the refractive index according to the Maxwell Garnett relationship (open circles). Solid line is derived from data in Fig. 12a. according to Eq. (20). From Brinker et al.[37]

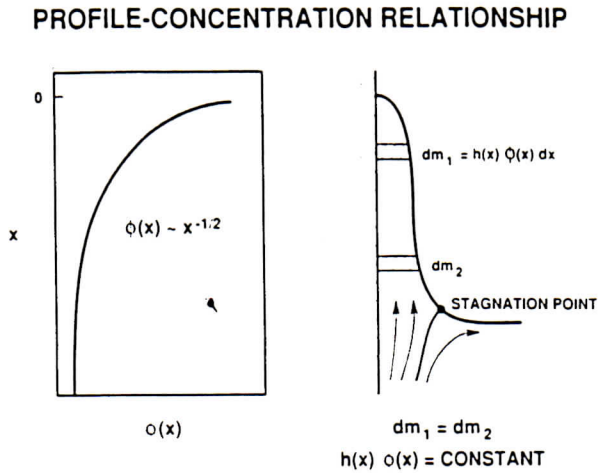

Fig. 13a. Fluid profile-concentration relationship for sol-gel dip-coating according to Eq. (20). From Hurd.[61]

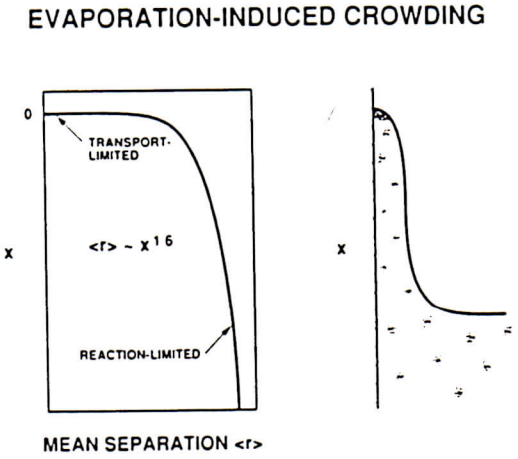

Fig. 13b. Fluid profile-mean separation relationship during sol-gel dip-coating. From Hurd.[61]

precipitous function: half the distance between particle (polymer) neighbors is traveled in the last 2% of the deposition process (~0.1 s). This evaporation-driven transport may be viewed like that induced by centrifugation or electrophoresis: the centrifugal acceleration needed to cause an equivalent rate of crowding is as much as 10^6g![*7] Since rheological properties of suspensions are often concentration dependent,[64] the increasing concentration of the inorganic species is expected to alter the rheology from Newtonian (dilute conditions) to shear-thinning (aggregated systems) or thixotropic (ordered systems). The viscosity also exhibits concentration dependence, at least for high concentration. Bornside et al.,[63] in their studies of spin-coating, assumed the following relationship:

$$\eta = \eta_0(1-\chi_A)^4 + \eta_s \qquad (21)$$

where η is the viscosity of the sol, η_s is the viscosity of the solvent, η_0 is the viscosity of the polymer, and χ_A is the mass fraction of solvent. From this relationship, we see that the viscosity will change abruptly in the vicinity of the drying line during dip-coating or during the evaporation stage of spin-coating.

The short time of the deposition process (~10 s) and, more importantly, the extremely short time in which the inorganic species are in close proximity ($\ll$1 s) establish important time scales for the dip- and spin-coating processes and distinguish sol-gel thin film formation from bulk (monolithic) gel formation. For bulk systems, the gelling sol is normally

*7 This assumes that there exists no steric barriers to concentration; often aggregation/network formation will interupt this dramatic compaction process.

the time required to prepare a monolithic bulk gel is on the order of days to weeks. During dip-coating (and spin-coating) the drying stage completely overlaps the gelation and aging stages. The depositing sol (which initially is often less concentrated than sols intended for bulk gels) remains rather dilute until the final stage of the deposition process at which point it is rapidly concentrated. There are only fractions of seconds available for condensation reactions (Eqs. (3) and (4)) to occur.

We anticipate several consequences of the short time scale of the film deposition process. (1) There is little time available for reacting species to "find" low energy configurations. Thus (for reactive systems) the dominant aggregative process responsible for network formation may change from reaction-limited (near the reservoir surface) to transport-limited near the drying line (see, Fig. 13b). The reduced fractal dimensionality of transport-limited aggregates should result in more porous networks (see, Eq. (8)). (2) For sols composed of repulsive particles, there is little time available for the particles to order as they are concentrated in the thinning film. (3) There is little time available for condensation reactions to occur. Thus gelation may actually occur by a physical process, through the concentration dependence of the viscosity (e.g., Eq. (21)), rather than a chemical process. (In some systems this is evident by the fact that the deposited film is quickly re-solubilized when immersed in solvent.) (4) Since the gels are most likely weakly condensed compared to bulk gels, they are more easily compacted; first by evaporation and then by the capillary pressure exerted at the final stage of the deposition (drying) process (see, Fig. 5a). Furthermore the maximum capillary pressure is likely to be higher due to the collapse of the network (and hence reduction in pore size) that precedes the final stage of drying. Of course, greater capillary pressure also promotes greater compaction of films compared to bulk gels.

4. Control of film microstructure

From the preceding discussion we expect that the final film structure should depend on the competition between such phenomena as evaporation and capillary pressure, which tend to compact the structure, and condensation reactions and aggregation processes which tend to stiffen the structure, resisting its tendency to collapse. In this section we document how these factors, along with the structure of the entrained inorganic species, influence film microstructure.

We characterize the film microstructure (surface area, % porosity, and pore size distribution) *in situ* by analyzing N_2 adsorption-desorption isotherms acquired using a surface acoustic wave (SAW) technique developed by Frye and co-workers.[14] The film is deposited on a piezoelectric quartz substrate (see, Fig. 14) which acts as a feedback element of an oscillator circuit. The substrate contains two sets of interdigital transducers; the application of an alternating field produces alternating strain, launching a surface acoustic wave. Changes in the mass of the film due to N_2 adsorption or desorption cause a change in the SAW velocity which is sensed as a change in the resonant frequency of the oscillator circuit. The extreme sensitivity of the SAW device (~80 pg/(cm^2 film)) permits accurate adsorption data to be obtained easily on a 1 cm^2 area of film less than 100 nm thick.

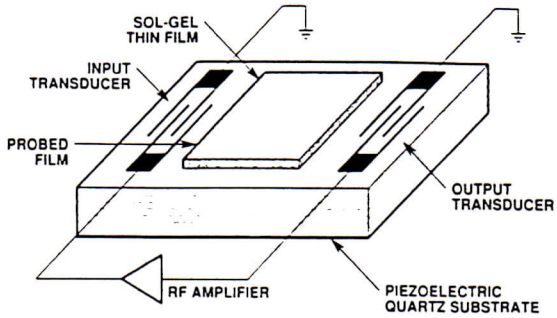

Fig. 14. Schematic illustration of surface acoustic wave (SAW) apparatus used to acquire gas adsorption-desorption data from sol-gel thin films.

4.1 Influence of precursor structure and reactivity

The possible structures of the inorganic precursors range from weakly branched polymers to highly condensed particles (see, e.g., Fig. 1).[65] For fractal objects the packing efficiency (i.e., the volume fraction solids, ϕ) depends on the fractal dimension, size, and condensation rate. The fractal dimension and size dictate steric constraints. Mandelbrot[56] has shown that if two structures of radius R are placed independently in the same region of space, the mean number of intersections $M_{1,2}$ is expressed as:

$$M_{1,2} \propto R^{D_1+D_2-d} \qquad (22)$$

where D_1 and D_2 are the respective fractal dimensions and d is the dimension of space ($d=3$). Thus if each object has a fractal dimension less than 1.5, the probability of intersection decreases indefinitely as R increases. These structures are mutually transparent: during film formation, they should freely interpenetrate as they are forced into close proximity by the increasing concentration. Alternatively, if the fractal dimension of each object exceeds 1.5, the probability of intersection increases algebraically with R. The structures, though porous, are mutually opaque; when concentrated they are unable to interpenetrate, much like an assemblage of "tumble-

weeds".

These concepts of mutual opacity or transparency assume that every intersection results in irreversible "sticking"; conditions chemically equivalent to an infinite condensation rate. In fact, the condensation rates of silicates are quite low (e.g., 10^{-4} 1/mole-sec)[66] and very dependent on $[H^+]$ (see, Fig. 2).[47),48)]. Thus the probability of sticking at any point of intersection is $\ll 1$, causing film structures to be generally more compact than expected from Eq. (22). For example, deposition of rather weakly branched silicate sols with $D=1.9$ (see, sample (b) in Fig. 3 and sample (A) in Fig. 4) at ~pH 2, where the condensation rate is minimized, produces dense films characterized by a Type II N_2 adsorption-desorption isotherm (see, Fig. 15b)[67] and surface area equivalent to the geometric area of the film.[14] This indicates that there is no porosity accessible to molecules larger than 0.4 nm, the kinetic diameter of the N_2 molecule. Because the condensation rate is low under these conditions, we expect that, although $D>1.5$, the precursors can interpenetrate as they are concentrated on the substrate surface by evaporation, leading to densely packed, but compliant, configurations with molecular-scale pores. During the final stage of drying the capillary pressure is enormous due to the small pores (Eq. (19)), causing further compaction of the compliant network.

The differences in time scales of bulk and thin film sol-gel processing are evident from the comparison of adsorption-desorption isotherms of the film and bulk xerogel (dried gel) prepared from identical silicate precursors (Fig. 15). Whereas the film is characterized by a Type II isotherm and low surface area, indicating no accessible porosity, the bulk xerogel isotherm (Fig. 15a) is of Type I, indicative of a microporous material, and the N_2 BET surface area exceeds 800 m^2/g. The long duration of the gelation, aging, and drying stages inherent in the bulk gel process allows the structure to stiffen at an early point of the drying stage through continued condensation reaction: the result is the gel is compacted less by evaporation during the initial stage of drying, so the pores are larger and the capillary pressure smaller (Eq. (19)) during the final stage of drying. Both increased stiffness and reduced capillary pressure cause the bulk sample to be much more porous than the film.

The interplay between precursor structure and condensation rate is well illustrated by a series of films prepared from more highly branched fractal clusters characterized by $D=2.4$ and a higher $Q_4/(Q_2+Q_3)$ ratio (see, sample (c) in Fig. 3).[17] Figure 16 shows that dip-coating at pH ≈ 3.5, where the con-

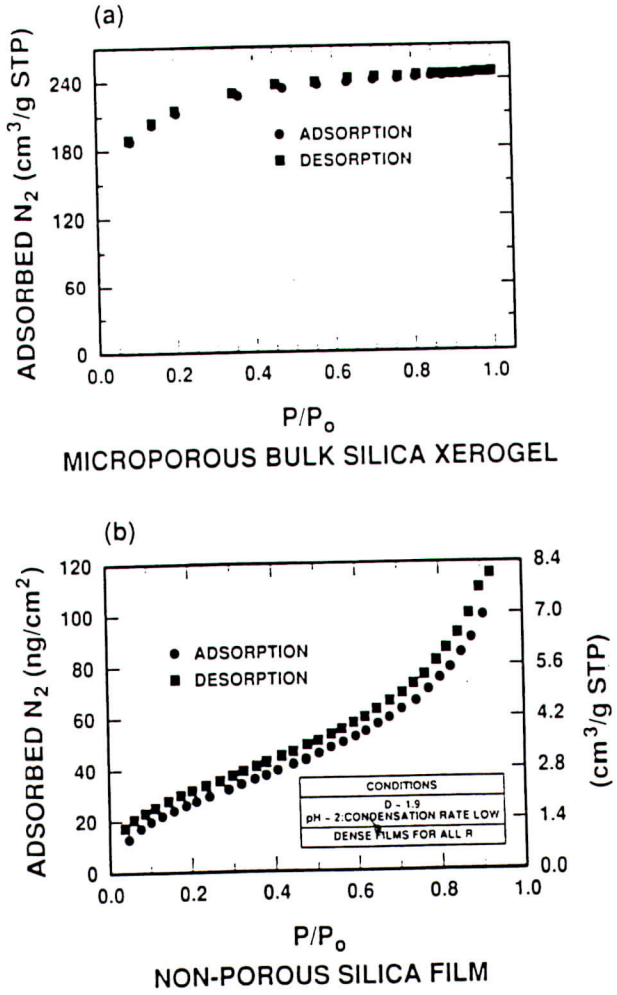

Fig. 15a. Type I N_2 adsorption-desorption isotherm for a bulk silica xerogel prepared from TEOS using a two-step acid-catalyzed process ($H_2O/Si=5$). From Brinker et al.[37]

Fig. 15b. Type II N_2 adsorption-desorption isotherm (acquired by SAW technique) for a silicate film prepared from the identical sol as in Fig. 15a. From Frye et al.[14]

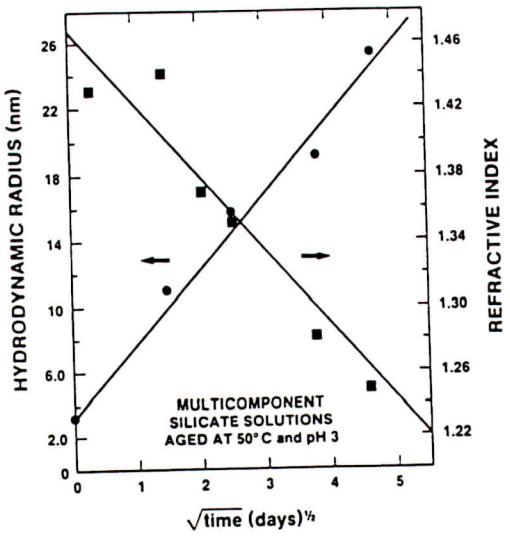

Fig. 16. Reciprocal relationship between the hydrodynamic radius of multicomponent silicate clusters ($D=2.4$) deposited near pH 3 and the corresponding refractive indices of the deposited films. Time refers to the aging times at 50°C and pH 3 employed to grow the inorganic clusters prior to film deposition. From Brinker et al.[17]

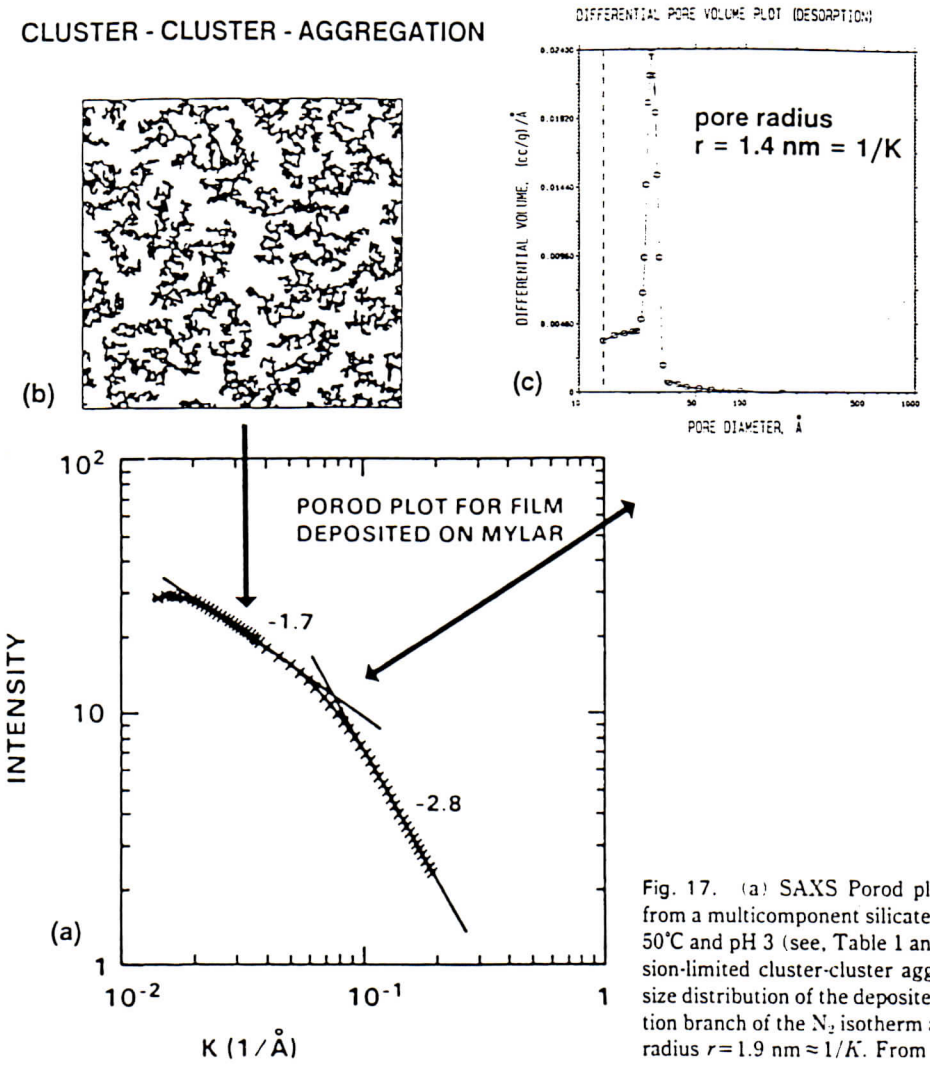

Fig. 17. (a) SAXS Porod plot for film deposited on MYLAR from a multicomponent silicate sol after about two weeks aging at 50°C and pH 3 (see, Table 1 and Fig. 16). (b) Simulation of diffusion-limited cluster-cluster aggregation. (c) Corresponding pore size distribution of the deposited film determined from the desorption branch of the N_2 isotherm acquired by SAW techniques. Pore radius $r = 1.9$ nm $\approx 1/K$. From Brinker and Scherer.[40]

densation rate is high (see, Fig. 2), produces films exhibiting a reciprocal relationship between refractive index (proportional to ϕ) and polymer (cluster) size prior to film deposition (determined by quasi-elastic light scattering).[17] Since the density of a fractal object decreases as $1/R^{(3-D)}$, this behavior appears consistent with an assemblage of mutually opaque clusters: high values of D and the condensation rate preclude interpenetration of large clusters, so the density (refractive index) of an assemblage of opaque clusters also decreases with R. Smaller clusters are both more dense (Eq. (8)) and, according to Eq. (22), less opaque leading to denser films.[*8]

Corresponding SAXS data are consistent with this fractal viewpoint. Figure 17 shows a Porod plot for a film deposited on MYLAR from a precursor sol ($D \approx 2.4$) aged about two weeks at 50°C and pH 3.5 before coating. Two limited power-law regions are indicated with a crossover at $1/K \approx 1.9$ nm. On length scales shorter than 1.9 nm, $P = -2.8$, corresponding to $D = 2.8$, whereas on longer scales, $P = -1.7$, corresponding to $D = 1.7$. These data suggests that the

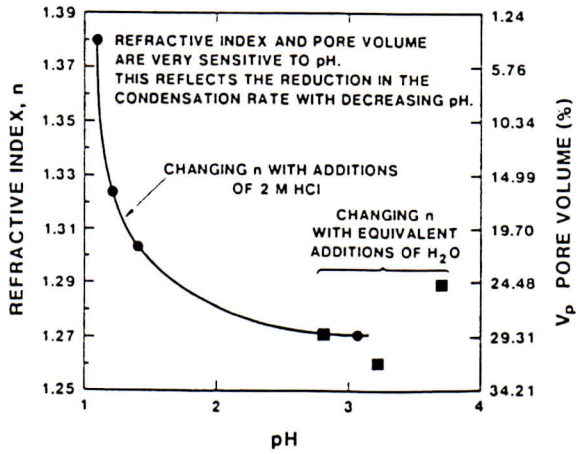

Fig. 18. Refractive index and pore volume of films prepared from multicomponent silicate precursors ($D = 2.4$, aged at 50°C and pH 3 for two weeks before deposition) versus the deposition pH. pH was adjusted from an initial value of 3.2 by addition of 2 M HCl. Changes in the refractive index caused by equivalent volumes of water are indicated by boxes. From Brinker et al.[57]

[*8] Eq. (8) indicates that the density of an individual cluster decreases with decreasing D; however Eq. (22) implies that the extent of interpenetration of aggregating fractals increases (density increases) with decreasing D. Since the film is formed by aggregation of individual clusters, the film density generally reflects the density of the aggregate rather than that of the individual cluster.

Table 1. Refractive index, % porosity, pore size, and surface area of films versus sol aging times prior to film deposition.

PROMISING APPLICATIONS ARE CONTROLLED PORE SIZE FILMS FOR SENSORS, MEMBRANES, OPTICS, ELECTRONICS, AND PROTECTION

MICROSTRUCTURAL TAILORING OF SOL-GEL FILMS

Sample Aging Times *	Refractive Index	% Porosity†	Median Pore Radius (nm)	Surface Area m^2/g	Applications
Unaged	1.45	0	<0.2	1.2 - 1.9	dense protective, electronic and optical films
0-3 Days					microporous films for sensors and membranes
3 Days	1.31	16	1.5	146	mesoporous films for sensors, membranes, catalysts, optics
1 Week	1.25	24	1.6	220	
2 Week	1.21	33	1.9	263	
3 Week††	1.18	52	3.0	245	

* AGING OF DILUTE SOL AT 50 C AND pH3 PRIOR TO FILM DEPOSITION.
† DETERMINED FROM N_2 ADSORPTION ISOTHERM.
†† THE 3 WEEK SAMPLE GELLED. IT WAS RE-LIQUIFIED AT HIGH SHEAR RATES AND DILUTED WITH ETHANOL PRIOR TO FILM DEPOSITION

original polymeric clusters aggregate by a diffusion-limited process ($D=1.7$) as they are rapidly concentrated at the final stage of the deposition step (see, Fig. 13). The individual clusters are then partially collapsed by the capillary pressure created by the tiny menisci, causing D to increase on short length scales. The crossover occurs at a value of $1/K$ approximately equal to the pore radius determined from the desorption branch of the corresponding N_2 isotherm.

From Table 1[37] we see that all of the important structural properties (% porosity, pore size, surface area and refractive index) of this series of films may be controlled by the aging (growth) step prior to film deposition. This allows the films to be tailored to specific applications such as protective coatings, membranes, sensor surfaces, or catalyst supports. Figure 18 illustrates that a progressive reduction in the condensation rate during deposition (via a reduction in the pH of the sol immediately prior to deposition) causes a corresponding increase in the refractive index (increase in ϕ) of films prepared from precursors aged 2 weeks at pH 3 prior to dip-coating.[57] Although $D \gg 1.5$, the reduction in the condensation rate promotes interpenetration and retards stiffening leading to denser films. This system demonstrates that microstructural tailoring may be accomplished by controlling the size and structure of the polymeric precursors or their rates of condensation (or both)!

4.2 Effects of capillary pressure and aging during deposition

In sol-gel processing of silicon alkoxides, the hydrolysis step has been carried out with H_2O:Si ratios exceeding 50. Since water is produced by condensation, a H_2O/Si ratio of 2 is theoretically sufficient to achieve complete hydrolysis and condensation of $Si(OR)_4$ to form SiO_2. Even if no condensation occurs, $H_2O/Si>4$ results in "excess" water. Thus whenever $Si(OR)_4$ is dissolved in alcohol and hydrolyzed with H_2O/Si ratios exceeding 4, there will always be excess water in the precursor sol.

As discussed in Section 2, one consequence of excess water is water enrichment in the vicinity of the drying line due to preferential evaporation and surface tension gradient driven flows. This causes a corresponding increase in the capillary pressure (due to

EFFECT OF PORE FLUID COMPOSITION

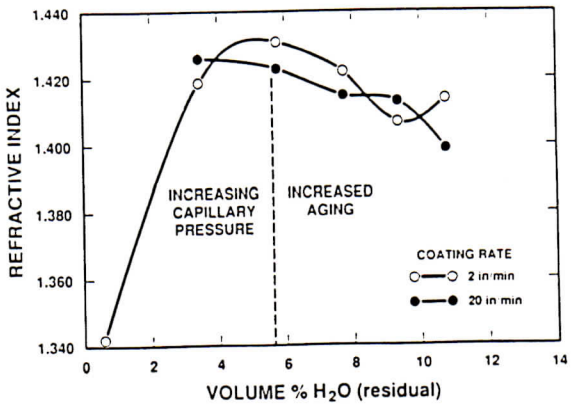

Fig. 19. Refractive index of silicate films versus the volume of residual (excess) water present in the coating sol, assuming $n\mathrm{Si(OR)_4}+2n\mathrm{H_2O}\rightarrow n\mathrm{SiO_2}+2n\mathrm{ROH}$. From Brinker et al.[37]

the film interior (see, Fig. 5a and Eq. (19)). Assuming complete wetting ($\theta=0°$ in Eq.(19)), the maximum increase in pressure would be a factor of ~3.

In order to evaluate the effect of water enrichment on the structure of the deposited film, we prepared silicate sols in which excess water was varied from about 0.5 to 10.5 vol % (assuming complete hydrolysis and condensation). The refractive index of the deposited films increased from 1.342 to 1.431 as the excess water was increased from 0.5 to 6 vol % (see Fig. 19), corresponding to a reduction in porosity from 22 to 7%. Further increases in the excess water caused a reduction in refractive index (increase in porosity). We believe that this behavior reflects the competition between capillary pressure and aging (stiffening) of the silicate skeleton, which are both enhanced by the increasing water concentrations. These results differ from those of Glaser and Pantano[68] who observed a monotonic increase in refractive index with water concentration for spin-coated silicate films. The difference between dip- and spin-coating is the evaporation rate and correspondingly the time available for aging. Spinning creates a strong forced convection in the vapor above the substrate,[38] increasing the evaporation rate. Thus there is little time for aging to occur, and the structure of the film is dominated by the effects of capillarity.

4.3 Effect of substrate speed

An increase in the substrate speed U_0 results in an increase in film thickness according to Eqs. (9) and (10). Since virtually all solvent evaporation occurs at the exterior surface of the entrained sol (i.e., at the sol-vapor interface), thicker films take longer to dry, increasing the aging time for reactive sols and, as we shall see, the time for ordering of repulsive sols. A second effect of the substrate speed is the shear field induced within the depositing sol. When the effects of shear experienced by a particle over-

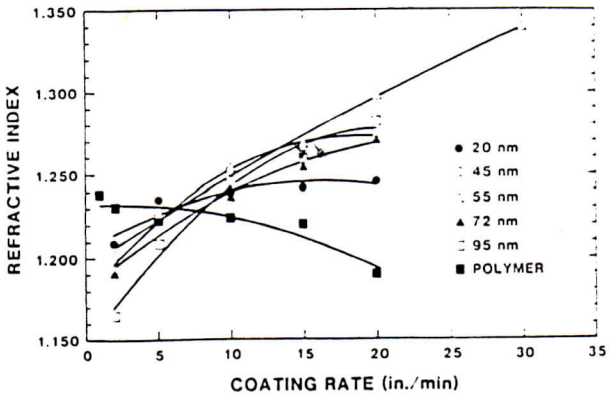

Fig. 20. Refractive index versus withdrawal speed for silicate films deposited from repulsive, monosized, particulate sols at ~ pH 11 compared to films prepared from reactive polymeric sols (see, Table 1 and Fig. 16) at ~pH 3. From Brinker et al.[17]

ed planes oriented parallel to the substrate surface or that asymmetrically shaped particles might align with their long axes parallel to the shear field.

Figure 19 plots refractive index versus U_0 for a series of monosized, particulate sols deposited at ~ pH 11 where deprotonation of surface silanols causes the particles to experience a uniform electrostatic repulsion (condensation rate ≈ 0). Also plotted is the refractive index–U_0 relationship for a reactive, polymeric sol deposited near pH 3 (sol system described by Table 1 and Fig. 16) where the polymers are more weakly charged and the condensation rate is high. For all sizes of repulsive particles, we observe a monotonic increase in refractive index with increasing U_0. The opposite relationship is observed for the reactive, polymeric sol.

Nitrogen adsorption-desorption isotherms acquired for the 55 nm particulate sols by SAW techniques show that the volume fraction porosity decreases from 36 to 26% as the coating rate is increased from 12.7 to 45.7 cm/min. For packings of monosized spherical sols, this corresponds to a change from random dense packing (consistent with a liquid-like structure observed in previous SAXS experiments[17]) to face centered cubic (or hexagonal) close packing. Thus we infer that increased coating rates result in particle ordering.

The smooth increase in refractive index with U_0 argues against a discrete phase transition from a liquid-like to a crystal-like structure. Experiments on monosized, spherical, colloids[69] at constant concentration, however, indicate such a transition when $\phi \approx 0.3$ and the Peclet number (Pe, a dimensionless parameter reflecting the relative rates of shear and diffusion):

$$Pe = \omega a^2 / D_0 \qquad (23)$$

exceeds about 1, where ω equals the shear rate (sec^{-1}), a equals the particle diameter (cm), and D_0 equals the diffusion coefficient ($cm^2 \cdot sec^{-1}$). For 55 nm diameter particles deposited at 45.7 cm/min from a low viscosity alcohol-based sol, we calculate $Pe \approx 0.04$ near the liquid bath surface where ω is maximized (~275 sec^{-1}) for a *pure fluid*. This value is obviously too low to account for ordering. However according to the previous discussion of the deposition of sols from binary fluid mixtures, both the shear rate and sol viscosity are expected to be maximized in the vicinity of the drying line due to water enrichment, surface-tension-gradient-driven flows, and the concentration dependence of viscosity. These combined factors probably cause Pe to exceed 1 there. We note that, to date, preliminary light scattering experiments have not provided any direct evidence of ordering within the depositing sol, although we may not have the necessary spatial resolution to acquire data sufficiently close to the drying line where we anticipate ordering to occur.

A second consequence of increased withdrawal speeds is increased drying time. Increased time may benefit the ordering of repulsive particles, because finite time is required for alignment and registration of the particles into a crystal-like structure. Conversely, for the reactive sol, increased drying times caused increased stiffening of the silicate skeleton (aging) prior to the final stage of drying, leading to more porous films. In both cases the coating rate can be used to tune the porosity of the deposited film.

5. Summary

During sol-gel dip-coating, inorganic precursors are rapidly concentrated on the substrate surface by gravitational draining with concurrent evaporation and condensation reactions. We have presented examples of several factors that influence the structure of the deposited films: (1) size and opacity of fractal precursors; (2) relative rates of condensation and evaporation; (3) capillary pressure; (4) shear resulting from surface-tension-gradient-driven-flows; and (5) substrate withdrawal speed. By control of these factors it is possible to tailor the pore size, surface area, pore volume and refractive index of the deposited film for applications ranging from dense protective or passivation layers to films with precisely controlled pore sizes for sensor surfaces and separation membranes.

Acknowledgments The authors thank Roger Assink for many of the NMR spectra supplied and Dale Schaefer, Keith Keefer, and Ed Vernon for light and X-ray scattering results.

References

1) W. Geffcken and E. Berger, Deutsches Reichspatent 736411, May 6, 1939, assigned to Jenaer Glaswerk Schott & Gen., Jena.
2) H. Dislich, "Sol-Gel Technology for Thin Films, Fibers, Preforms, Electronics, and Specialty Shapes", L. C. Klein, Ed., Noyes, Park Ridge, NJ (1988) pp. 50-79.
3) H. Schroeder, "Physics of Thin Films, Vol. 5", Ed. G. Haas, Academic Press, NY (1969) pp. 87-141.
4) R. L. Nelson, J. D. F. Ramsay, J. L. Woodhead, J. A. Cairns and J. A. A. Crossley, *Thin Solid Films*, 81, 329-37 (1981).
5) D. P. Partlow and T. W. O'Keeffe, *Appl. Optics*, 29, 1526-29 (1990).
6) H. G. Floch, J.-J. Priotton and I. M. Thomas, *Thin Solid Films*, 175, 173-78 (1989).
7) B. E. Yoldas, *Appl. Optics*, 19, 1425-29 (1980).
8) A. Makishima, N. Kubo, K. Wada, Y. Kitami and T. Shimohira, *J. Am. Ceram. Soc.*, 69, C127-29 (1986).
9) B. E. Yoldas and D. P. Partlow, *Thin Solid Films*, 129, 1-14 (1985).
10) B. E. Yoldas, *Appl. Optics*, 21, 2960-64 (1982).
11) R. B. Pettit and C. J. Brinker, *SPIE Optical Coatings for Energy Efficiency and Solar Applications*, 324, 176 (1982).
12) W. L. Warren, P. M. Lenahan, C. J. Brinker, G. R. Shaffer, C. S. Ashley and S. T. Reed, "Better Ceramics Through Chemistry IV", Eds. B. J. J. Zelinski, C. J. Brinker, D. E. Clark, and D. R. Ulrich, Mat. Res. Soc. Symp. Proc., Vol. 180, Mat. Res. Soc., Pittsburgh, PA (1990) pp. 413-19.
13) C. S. Ashley, S. T. Reed and A. R. Mahoney, "Better Ceramics Through Chemistry III", Eds. C. J. Brinker, D. E. Clark, and D. R. Ulrich, Mat. Res. Soc. Symp. Proc., Vol. 121, Mat. Res. Soc., Pittsburgh, PA (1988) pp. 635-38.
14) G. C. Frye, A. J. Ricco, S. J. Martin and C. J. Brinker, "Better Ceramics Through Chemistry III", Eds. C. J. Brinker, D. E. Clark, and D. R. Ulrich, Mat. Res. Soc., Pittsburgh (1988) pp. 349-54.
15) T. Bein, G. C. Frye and C. J. Brinker, *J. Am. Chem. Soc.*, 111, 7640-41 (1989).
16) R. B. Pettit, C. J. Brinker and C. S. Ashley, *Solar Cells*, 15, 267-78 (1985).
17) C. J. Brinker, A. J. Hurd and K. J. Ward, "Ultrastructure Processing of Advanced Ceramics", J. D. Mackenzie and D. R. Ulrich, Eds., Wiley, NY (1988) p. 223.
18) A. F. M. Leenaars, K. Keizer and A. J. Burggraaf, *J. Mater. Sci.*, 10, 1077-88 (1984).
19) M. A. Anderson, M. J. Geiselmann and Q. Xu, *J. Membrane Sci.*, 39, 243-58 (1988).
20) D. P. Partlow and J. Greggi, *J. Mat. Res.*, 2, 595-605 (1987).
21) S. Hirano and K. Kato, *Adv. Ceram. Mat.*, 3, 503-06 (1988).
22) S. Hirano and K. Kato, *J. Non-Cryst. Solids*, 100, 538 (1988).
23) J. Livage and J. Lemerle, *Ann. Rev. Mat. Sci.*, 12, 103-22 (1982).
24) P. Baundy, A. C. M. Rodrigues, M. A. A. Aergerter and L. O. Bulhoes, *J. Non-Cryst. Solids*, 121, 319-22 (1990).
25) S. A. Kramer, G. Kordas, J. McMillan, G. C. Hilton and D. J. Van Harligen, *Appl. Phys. Lett.*, 53, 156-58 (1988).
26) B. D. Fabes, W. F. Doyle, B. J. J. Zelinski, L. A. Silverman and D. R. Uhlmann, *J. Non-Cryst. Solids*, 82, 349 (1986).
27) B. D. Fabes and G. D. Berry, *J. Non-Cryst. Solids*, 121, 357-64 (1990).
28) K. D. Budd, S. K. Dey and D. A. Payne, Brit. Ceram. Proc., 36(1985) pp. 107-122.
29) J. Fukushima, K. Kodaira and T. Matsushita, *J. Mater. Sci.* 595-58 (1984).
30) U. Brautigam, H. Burger and W. Vogel, *J. Non-Cryst. Solids*, 110, 663-69 (1989).
31) D. I. Butts, W. C. LaCourse and S. Kim, *J. Non-Cryst. Solids*, 110, 514-18 (1988).
32) H. Schmidt, G. Rinn, R. Nass and D. Sporn, "Better Ceramics Through Chemistry III", Eds. C. J. Brinker, D. E. Clark and D. R. Ulrich, Mat. Res. Soc. Symp. Proc., Vol. 121, Mat. Res. Soc. Pittsburgh, PA (1988) pp. 743-54.
33) F. Orgaz and F. Capel, *J. Mater. Sci.*, 22, 1291-94 (1987).
34) S. M. Melpolder and B. K. Coltrain, "Better Ceramics Through Chemistry III", Eds. C. J. Brinker, D. E. Clark and D. R. Ulrich, Mat. Res. Soc. Symp. Proc., Vol. 121, Mat. Res. Soc., Pittsburgh, PA (1988) pp. 811-16.
35) I. Strawbridge and P. F. James, *J. Non-Cryst. Solids*, 86, 381-93 (1986).
36) M. Guglielmi and S. Zenezini, *J. Non-Cryst. Solids*, 121, 303-09 (1990).
37) C. J. Brinker, A. J. Hurd, G. C. Frye, K. J. Ward and C. S. Ashley, *J. Non-Cryst. Solids*, 121, 294-302 (1990).
38) L. E. Scriven, "Better Ceramics Through Chemistry III", C. J. Brinker, D. E. Clark and D. R. Ulrich, Eds., Mat. Res. Soc. Symp. Proc., Vol. 121, Mat. Res. Soc., Pittsburgh, PA (1988) pp. 717-29.
39) A. J. Hurd and C. J. Brinker, *J. de Physique*, 49, 1017-25 (1988).
40) C. J. Brinker and G. W. Scherer, "Sol-Gel Science", Academic Press, San Diego (1990).
41) B. E. Yoldas, *Am. Ceram. Soc. Bull.*, 54, 286-90 (1975).
42) J. H. A. Van Der Woude and P. O. DeBruyn, *Colloids and Surfaces*, 12, 79 (1984).
43) A. Bleier and R. M. Cannon, "Better Ceramics Through Chemistry II", Eds. C. J. Brinker, D. E. Clark and D. R. Ulrich, Mat. Res. Symp. Proc., Vol. 73, Mat. Res. Soc., Pittsburgh, PA (1986) p. 71.
44) J. Livage, M. Henry and C. Sanchez, *Prog. in Solid State*

Chem., 18, 259–342 (1988).
45) J. L. Hall, W. E. Dean and E. A. Pacofsky, *J. Am. Chem. Soc.*, 82, 3303 (1960).
46) Y. Takahashi and Y. Wada, *J. Electrochem. Soc.*, 137, 267–72 (1990).
47) R. K. Iler, "The Chemistry of Silica", Wiley, NY (1978).
48) B. K. Coltrain, S. M. Melpolder and J. M. Salva, The Proceedings of the IVth International Conference on Ultrastructure Processing of Glasses, Geramics and Composites", Feb. 19–24, 1989, Tucson, AZ, Eds. D. R. Uhlmann and D. R. Ulrich, Wiley, NY, to be published (1991).
49) L. W. Kelts and N. J. Armstrong, "Better Ceramics Through Chemistry III", Eds. C. J. Brinker, D. E. Clark and D. R. Ulrich, Mat. Res. Soc. Symp. Proc., Vol. 121, Mat. Res. Soc., Pittsburgh, PA (1988) p. 519.
50) J. L. Lippert, S. B. Melpolder and L. W. Kelts, *J. Non-Cryst. Solids*, 104, 139–47 (1988).
51) L. W. Kelts, N. J. Effinger and S. M. Melpolder, *J. Non-Cryst. Solids*, 83, 353–74 (1986).
52) J. E. Martin and A. J. Hurd, *J. Appl. Cryst.*, 20, 61–78 (1987).
53) D. W. Schaefer, *MRS Bulletin*, 8, 22–27 (1988).
54) D. W. Schaefer and K. D. Keefer, "Fractals in Physics", Eds. L. Pietronero and E. Tosatti, North-Holland, Amsterdam (1986) pp. 39–45.
55) P. Meakin, *Phys. Rev. Lett.*, 51, 1119 (1983).
56) B. B. Mandelbrot, "The Fractal Geometry of Nature", Freeman, San Francisco (1982).
57) C. J. Brinker, G. C. Frye, A. J. Hurd and C. S. Ashley, "Fundamentals of Sol-Gel Dip-Coating", Thin Solid Films, in press.
58) L. D. Landau and B. G. Levich, *Acta Physiochim., USSR*, 17, 42–54 (1942).
59) S. D. R. Wilson, *J. Eng. Math*, 16, 209 (1982).
60) A. J. Hurd and C. J. Brinker, "Better Ceramics Through Chemistry IV", B. J. J. Zelinski, C. J. Brinker, D. E. Clark, D. R. Ulrich, Eds., Mat. Res. Soc. Symp. Proc., Vol. 180, Mat. Res. Soc., Pittsburgh, PA (1990) pp. 575–81.
61) A. J. Hurd, " The Colloidal Chemistry of Silica", Ed. H. Bergna (ACS Adv. in Chem. Series, in press).
62) P. R. Schunk, A. J. Hurd and C. J. Brinker, "Dip Coating of Sol Gels", in Proceedings of the 44th Annual Conf. of the Soc. of Imaging Science and Tech., St. Paul, MN, May 12–17 (1991).
63) D. E. Bornside, C. W. Macosko and L. E. Scriven, *J. Appl. Phys.*, 66, 5185–93 (1989).
64) S. Sakka and K. Kamiya, *J. Non-Cryst. Solids*, 48, 31–46 (1982).
65) C. J. Brinker, K. D. Keefer, D. W. Schaefer, R. A. Assink, B. D. Kay and C. S. Ashley, *J. Non-Cryst. Solids*, 63, 45–59 (1984).
66) M. F. Bechtold, W. Mahler and R. A. Schunn, *J. Polym. Sci., Polym. Ed.*, 18, 2823 (1980).
67) S. J. Gregg and K. S. W. Sing, "Adsorption Surface Area, and Porosity", Academic Press, NY (1982).
68) P. M. Glaser and C. G. Pantano, *J. Non-Cryst. Solids*, 63, 209–21 (1984).
69) B. J. Ackerson, *J. of Rheology*, 34, 553 (1990).

C. Jeffrey BRINKER

Alan J. HURD

Gregory C. FRYE

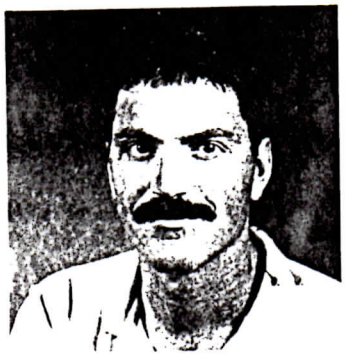

P. R. SCHUNK

Carol ASHLEY

C. Jeffrey BRINKER received his B. S., M. S., and Ph. D. degrees from Rutgers University, New Brunswick, NJ. He joined the Ceramic Development Division at Sandia National Laboratories as a member of the technical staff in 1979, where he initiated a program in sol-gel processing of ceramics. Today Brinker is a Distinguished Member of the Technical Staff (Inorganic Materials Chemistry Division) and a University of New Mexico/Sandia National Laboratory Distinguished Professor of Chemistry and Chemical Engineering. He is the recipient of the 1986 DOE Basic Energy Sciences Award for Sustained Outstanding Research in Metallurgy and Ceramics and the 1988 Zachariasen Award for best contributions to the glass science literature (1985-87). He was named Fellow of the American Ceramic Society in 1990. Brinker in the author or co-

author of over 90 papers and the editor of 4 books. He and co-author George Scherer recently completed a book entitled, "Sol-Gel Science: The Physics and Chemistry of Sol-Gel Processing", published by Academic Press in March 1990.

Alan J. HURD was educated at Colorado School of Mines (B. S., Physics, 1976) and the University of Colorado (M. S., Ph. D., Physics, 1981) where he studied the lattice dynamics of colloidal crystals. During the following three years at Brandeis University, first as a postdoc then as an assistant professor, he studied liquid crystal instabilities and two-dimensional colloidal systems. Since May of 1984, he has been a Member of the Technical Staff at Sandia National Laboratories and currently supervises the Interfacial Chemistry and Coatings Research Division. In recent years, his research interests have included sol-gel films, dip coating, fractals and aerosols, in which he has specialized in optical and scattering probes. He is a member of the American Physical Society, the American Association for Aerosol Research, and he is active locally and nationally in the Materials Research Society. He was born February 1, 1954, in Las Animas, Colorado, is married, and has 4 children.

Gregory C. FRYE received his B. S. degree from the University of Colorado and his Ph. D. from the University of Washington, both in Chemical Engineering. He is currently a Senior Member of Technical Staff in the Inorganic Materials Chemistry Division at Sandia National Laboratories. His main interests are in thin film materials, acoustic wave devices and chemical sensors. Specific research areas include using acoustic wave devices to characterize the surface area and pore size distribution of porous thin films, developing surface modified oxide coatings with tailored porosity for application as the discriminating element of chemical sensors, and development of environmental monitoring systems based on acoustic wave devices.

P. R. SCHUNK received a B. S. degree in Chemical Engineering from the University of Colorado at Boulder in 1984, and received a Ph. D. degree in Chemical Engineering from the University of Minnesota in 1989; his dissertation was entitled "Polymer and Surfactant additives in Coating and Related Flows". Currently working in the Department of Fluid, Thermal and Structural Sciences at Sandia National Laboratories in New Mexico, his research topics include specialty metals processing, sol-gel coating, and parallel computing.

Carol ASHLEY is a Member of the Technical Staff in the Inorganic Materials Chemistry Division at Sandia National Laboratories, Albuquerque, New Mexico. She has worked in sol-gel research and development since 1980 and has played a major role in sol-gel processing and applications, especially in the development of thin film processes for optics, planarization, dielectrics, and protection, as well as in the development of aerogel composite materials. She has co-authored over 20 publications and has seven patents awarded or pending in thin film and aerogel processing. She is a graduate of the University of New Mexico and was the recipient of a national American Chemical Society award in 1990.